Synergism of SeaWinds and AMSR

Editors

Naoto Ebuchi
Institute of Low Temperature Science, Hokkaido University
Sapporo, Japan

and

W. Timothy Liu
Jet Propulsion Laboratory, California Institute of Technology
Pasadena, California, U.S.A.

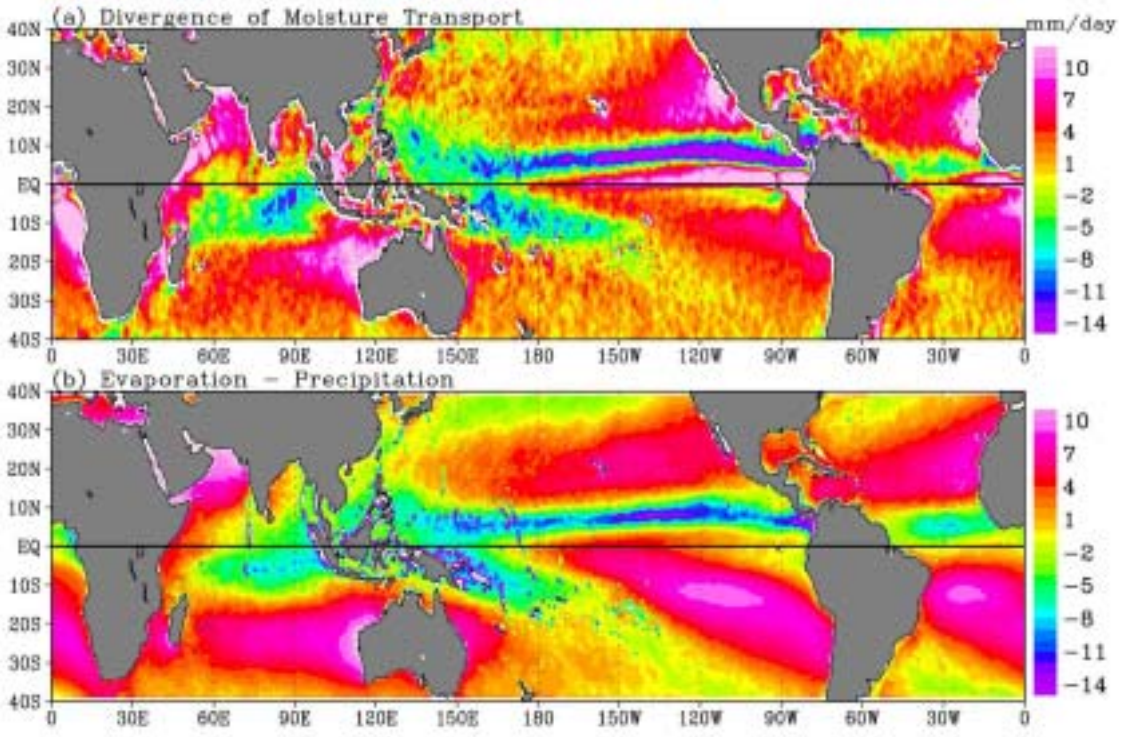

February 2005

About the Cover

Because of the conservation of mass, the divergence of the moisture transport integrated over the depth of the atmosphere should balance the fresh water flux (evaporation-precipitation) at the surface. Monitoring these two terms is critical to the characterization of the hydrological cycle and climate change. Direct in situ measurements of moisture transport, evaporation, and precipitation are extremely sparse over ocean. The three terms were estimated independently using spaceborne microwave scatterometer and radiometers and the similar geographical distribution, as shown in the figure, is one of the best validation of the estimation technique and a clear demonstration of the science synergism of the two instruments. (*courtesy of W. Timothy Liu, Xiaosu Xie, and Wenqing Tang*)

Synergism of SeaWinds and AMSR

Editors

Naoto Ebuchi
Institute of Low Temperature Science, Hokkaido University
Sapporo, Japan

and

W. Timothy Liu
Jet Propulsion Laboratory, California Institute of Technology
Pasadena, California, U.S.A.

February 2005

Synergism of SeaWinds and AMSR

Naoto Ebuchi[1] and W. Timothy Liu[2] (editors)

1 Institute of Low Temperature Science, Hokkaido University
2 Jet Propulsion Laboratory, California Institute of Technology

Contributors

Robert Atlas	Goddard Space Flight Center
Don Cavalieri	Goddard Space Flight Center
Rong Fu	Georgia Institute of Technology
Kyle Hilburn	Remote Sensing Systems
Keiji Imaoka	Japan Aerospace Exploration Agency
Masafumi Kamachi	Meteorological Research Institute
Masahisa Kubota	Tokai University
David Long	Brigham Young University
Son Nghiem	Jet Propulsion Laboratory
Eni Njoku	Jet Propulsion Laboratory
Akira Shibata	Earth Observation Research Center
Yoshiaki Takeuchi	Japan Meteorological Agency
Wenqing Tang	Jet Propulsion Laboratory
David Weissman	Hofstra University
Svetla Veleva	Jet Propulsion Laboratory
Shang-Ping Xie	University of Hawaii
Xiaosu Xie	Jet Propulsion Laboratory
Simon Yueh	Jet Propulsion Laboratory

ABSTRACT

A combination of spaceborn scatterometer and radiometer provides us with instantaneous observation of various physical parameters of air-sea interface, such as wind speed and direction, water vapor content, sea surface temperature (SST), and rain rate, which are essential to scientific studies of global climate changes. The combined observation also plays an important role in the operational applications, such as weather forecast and disaster prevention. The Japanese earth observation satellite, Advanced Earth Observing Satellite-II (ADEOS-II), which carried a microwave scatterometer, SeaWinds, and a microwave radiometer, Advanced Microwave Scanning Radiometer (AMSR), was launched by the National Space Development Agency of Japan (NASDA) in December 2002, and the simultaneous observation was started. However, ADEOS-II failed in October 2003. A follow-up mission is required to continue the data flow for the operational applications and scientific studies. The Japan Aerospace Exploration Agency (JAXA) is now proposing a new mission called Global Change Observation Mission-W (GCOM-W) that will carry a microwave scatterometer and radiometer. This mission will also offer unique opportunities to address key issues of the Earth Science Enterprise (ESE) at the National Aeronautics and Space Administration (NASA). The simultaneous operation of the active and passive microwave sensors will contribute to improve sensor algorithms to estimate physical parameters. The radiometer measurements will be used by the scatterometer for rain flagging and improving wind retrieval under rain. Scatterometer wind will be able to correct wind direction dependence of the radiometer measurements. The simultaneous observation of the water vapor, precipitation and marine surface vector winds will have a significant impact on studies of the water-energy cycle, which is one of the most important scientific topics and social issues. The mission will provide a unique data set to investigate the balance among horizontal convergence/divergence of the water vapor, evaporation from the sea surface, and precipitation. Monitoring these terms is critical to the characterization of the hydrological cycle and climate changes. The combined measurements of the vector wind, water vapor, SST, and rain will also help to monitor tropical climate including tropical convection systems and cloud clusters, the intertropical convergence zone (ITCZ), and the interannual climate anomalies of El Nino/Southern Oscillation (ENSO), which also influences the mid- and high-latitude climate variations. Scientific impacts of the mission will further extend to studies concerning various phenomena of the atmosphere and ocean, such as monsoon, tropical cyclones, ocean-atmosphere coupling mechanism, ocean's response to wind and hydrologic forcing, and operational numerical weather prediction, and also to cryospheric studies and land applications.

TABLE OF CONTENTS

1. Introduction

Progress of spaceborne microwave scatterometer and radiometer in these decades provide us with physical parameters of the air-sea interface, such as wind speed and direction, water vapor content, sea surface temperature, and rain rate, of calibrated accuracy, high spatial resolution and global coverage. The National Aeronautics and Space Administration (NASA) Scatterometer (NSCAT), which was carried by the Japanese earth observation mission, Advanced Earth Observing Satellite (ADEOS), opened up a new way of measuring ocean surface wind field and extended the horizon of operational applications and scientific investigations in 1996 (see Liu, 2002 for a review). A new scatterometer called SeaWinds on QuikSCAT has been intensively observing the global wind fields with high spatial and temporal coverages since 1999. On the other hand, the Tropical Rainfall Measuring Mission (TRMM) microwave imager (TMI) has proved high potential of microwave radiometers measuring water vapor, liquid water content, sea surface temperature (SST), and rain rate. Advanced Microwave Scanning Radiometer for Earth Observing System (AMSR-E) on Aqua has been providing us with multi-channel, dual-polarized passive microwave observations of earth's surface with high spatial resolution since 2002.

ADEOS-II, which carried SeaWinds and AMSR, was launched by the National Space Development Agency of Japan (NASDA) in December 2002, and simultaneous observation by the microwave scatterometer and radiometer was started. It was expected that the mission would prove high potential of the simultaneous operation of these two sensors in both aspects of sensor synergism and operational and scientific applications. However, ADEOS-II failed in October 2003. A follow-up mission is required to continue the data flow for operational applications and scientific studies relating to global climate changes.

The second Earth Observation Summit was held in Tokyo in April 2004, and the Framework for a 10-year implementation plan was adopted. In the implementation plan, it is required to establish new Global Earth Observation System of Systems (GEOSS). The implementation plan for launching GEOSS was endorsed at the third Earth Observation Summit held in Brussels in February 2005. Under these circumstances, the Japan Aerospace Exploration Agency (JAXA) is now proposing a new mission called Global Change Observation Mission-W (GCOM-W) that will carry a microwave scatterometer and radiometer (Furuhama, 2004). The GCOM is not a single satellite mission but consists of three consecutive satellites, lasting for more than a decade. The GCOM-W maintains the data flow for operational applications and scientific studies relating to global climate changes. This mission will also offer unique opportunities to address key issues of the NASA Earth Science Enterprise (ESE). This short report is intended to describe examples of highly likely opportunities and benefit offered by the GCOM-W mission carrying a microwave scatterometer and radiometer simultaneously from perspectives of experienced scientists.

In Section 2, technical concepts of the two sensors, an advanced wind scatterometer and AMSR Follow-on are described.

How will these sensors improve accuracy of retrieval of physical parameters by the other sensor? The radiometer measurements will be used by the scatterometer for rain flagging, corrections for the rain effects on the scatterometer signal, and improving wind retrieval under rain. Scatterometer wind will be able to correct wind direction dependence of the radiometer measurements. The sensor synergism is discussed in Section 3.

What are scientific benefits of the combination of the two sensors? Science synergism - science purpose combining two sensors- is discussed in Section 4.

The water-energy cycle is one of the most important scientific topics. Observations of water vapor, precipitation and surface winds from spacebased microwave radiometer and scatterometer can be applied to investigate the balance among horizontal convergence/divergence of the water vapor, evaporation from the sea surface, and precipitation. Monitoring these terms is critical to the characterization of the hydrological cycle and climate changes. An example of application to the water cycle is presented in Section 4.1.

Monsoon is the seasonal change of winds. The change is caused by the reversal of land-ocean temperature gradient. The oceanic influence is manifested through continental rain. Monsoons affect an extensive area of the world with large population. Their annual onset, intensity, and retreat vary greatly, and the variation has strong economic impact and may cause severe human suffering. An example of studies concerning oceanic influence on the precipitation in India using scatterometer and radiometer observations is presented in Section 4.2

Supply of water vapor from the sea surface and its convergence by the surface wind play important roles in growth of tropical cyclones. Simultaneous observation of vector wind, water vapor, liquid water content, SST, and rain by the scatterometer and radiometer will help to monitor tropical cyclones and understand their dynamics. Interplay between wind and rain in tropical cyclone is described in Section 4.3.

Interaction between atmosphere and ocean is one of key issues in the global climate system. The coordinated observation of vector wind, SST, and water vapor will help to understand the ocean-atmosphere coupling mechanism. Two examples of such air-sea feedback mechanism revealed using the combination of microwave scatterometer and radiometer are presented in Section 4.4.

The combined measurements of wind, water vapor, SST, and rain will help to monitor tropical convection systems and cloud clusters, such as the intertropical convergence zone (ITCZ), that lead to the intraseasonal westwind bursts, which are precursors to interannual climate anomalies of El Nino, and which may modify decadal mid-latitude temperature anomalies. Examples applying scatterometer and radiometer observations to the studies of the tropical climate are presented in Section 4.5.

Ocean's response to wind and hydrologic forcing can be investigated using ocean general circulation models with inputs from microwave radiometers and scatterometers. High resolution observations of the radiometers and scatterometers give significant impacts on the model results (Section 4.6).

The scatterometer-radiometer mission will provide a data set of vector wind, water vapor, SST, and precipitation with a high accuracy and global coverage. The data set will contribute to improve numerical weather prediction of the meteorological centers. How the scatterometer and radiometer observations will improve the operational analysis is described in Section 4.7.

In addition to the ocean and atmosphere, the simultaneous observation by the scatterometer and radiometer will be applied to cryosphere studies. Perspective for applications to sea ice and its snow cover and snow water equivalent on land are discussed in Section 4.8.

Active and passive signatures of Earth surfaces indicate sensitivities to common features, through the dielectric and geometric properties of the surface and subsurface media, though the relative sensitivities of the radar and radiometer to these properties may be quite different. Possible application of the combination of active and passive microwave sensors to land, such as soil moisture, freeze-thaw, and vegetation sensing, and flood monitoring, are summarized in Section 4.9.

2. Payload Concepts

2.1. Advanced Wind Scatterometer

The advanced wind scatterometer on the GCOM-W will be follow-on to SeaWinds scatterometers on the QuikSCAT and ADEOS spacecrafts to provide global ocean vector wind measurements. The objective is to enhance performance at low cost and low risk while extending the time series of ocean surface wind vector measurements. It should be a Ku-band co-pol scatterometer with SeaWinds coverage achieved by a 1800 km swath to meet the baseline requirements of QuikSCAT, whose original specification was for 3 to 30 m/s wind speeds with <2m/s speed and <20-degree direction accuracy.

The priority in performance enhancement are: (1) improve wind direction ambiguity removal skill, (2) mitigate errors caused by rain and atmospheric attenuation, (3) improve in resolution, (4) real time on-board processing and direct broadcasting of data.

It will include experimental polarimetric radar and radiometer channels to demonstrate the ability of unambiguous wind vector selection without external ancillary information and to explore the feasibility of extending the wind measurement capabilities to beyond 30 m/s wind speed and rainy conditions for the monitoring of tropical cyclones.

The instrument will feature a pencil-beam conical scanning Ku-band scatterometer with ability to measure the co-polarized radar echoes from oceans, similar to the SeaWinds scatterometer. The instrument electronics will have two receiving channels for simultaneous detection of the horizontally and vertically polarized echoes. The complex correlation of the two polarized echoes will be formed by on-board processor together with the nominal power measurements to achieve polarimetric information. The nominal power measurements will provide SeaWinds quality vector wind observations, while the complex correlation will reduce the number of ambiguous wind vector solutions or enhance the accuracy of selecting the closest wind vector solution.

The instrument concept will include a companion polarimetric radiometer channel for the correction of rain impact on scatterometer echoes and for providing complementary capability to augment the polarimetric radar channel for ambiguity removal. The combined active and passive polarimetric microwave measurements will also be used to develop the single-look microwave vector wind instrument for future operational satellites. To improve wind retrieval, at 10-km resolution, from range-compressed ‘slice’ data, slightly larger antenna and broader bandwidth are recommended. The key characteristics of the advanced wind scatterometer concept are summarized in Table 2.1.1.

New technology of combining scatterometer with along-track interferometer is being explored at the Jet Propulsion Laboratory (JPL), to measure both surface vector wind and ocean surface current at the same time. The decade long successive multi-mission deployment of GCOM-W would allow infusion of such new technology at a later stage. Our objective is always to lengthen the time series of consistent vector wind measurement while infusing new technology to expand the scientific applications.

Table 2.1.1. Key characteristics of the advanced wind scatterometer

Instrument function	Scatterometer	Radiometer
Frequency	13.4 GHz	18.7 GHz
Polarization	VV, HH, VH, and HV	All Stokes parameters (Tv, Th, U and V)
Antenna	Offset Parabolic Reflector with 2 m aperture	Share aperture with scatterometer
Spatial resolution	18 kmx10km with range compression	15kmx25km
Incidence angle	50 and 60 degrees	60 degrees
Swath Width	2000km	2000km
Antenna Scan Rate	20 RPM	Same
Radar transmit power	100W	NA
Radiometer NEDT (5 msec integration time)	NA	0.6K

2.2. AMSR Follow-on

The AMSR follow-on instrument will be a multi frequency, dual polarized passive microwave radiometer that observes water-related geophysical parameters supporting the GCOM concept. Conical scanning mechanism will be employed to observe the earth's surface with a constant incidence angle around 55 degrees. During each conical rotation, scene observation and calibration target measurements (warm and cold) will be made. The instrument will thus be calibrated once per scan by so-called two-point calibration. Momentum generated by rotating instrument will be compensated by an independent momentum wheel on the platform.

Brightness temperatures (Tb) of the ocean surface are influenced by various oceanic states including sea water emissivity, surface roughness, sea swell, white cap, and so on. These Tb responses (differ for different frequency and polarization) are used in estimating the oceanic geophysical parameters including sea surface wind speed and sea surface temperature. Other over-ocean parameters including water vapor, precipitation, and sea ice are also measured and will provide useful information in studying ocean-atmosphere interaction. Over land, snow water and soil moisture are observable.

After the ADEOS-II loss, the AMSR follow-on sensor team has been discussing desired follow-up activity to this accident. Since the AMSR-E on the EOS Aqua satellite has been still operational, the highest priority was given to the continuity of the AMSR-E observation that can provide high-spatial resolution and multi-channel microwave measurements. Therefore, the basic requirement is to launch the follow-on instrument that can take over the ADEOS-II AMSR performance and continue the AMSR-E

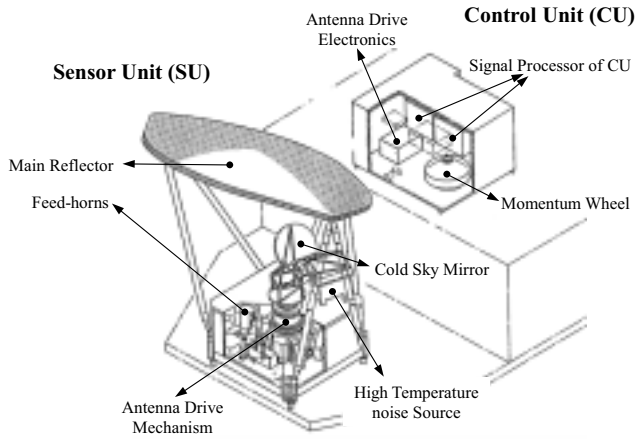

Figure 2.2.1. Overview of AMSR on ADEOS-II platform. AMSR is composed of two major units: the Sensor Units (SU) and Control Unit (CU).

observations. Schematic view of the AMSR instrument is shown in Figure 2.2.1. Also, major specifications are listed in Table 2.2.1.

To reduce the risks and keep the earliest launch date, minimum modification but with several essential improvements will be required. These include the improvement of the calibration system and some considerations to the C-band radio frequency interference (RFI) problem. As a whole, the AMSR instrument is well engineered system and scientists and data users are very satisfied with the massive improvements over the existing similar instruments. However, improving the calibration system including warm calibration target will be indispensable. Establishing the reliable calibration scheme is essential to the AMSR follow-on instrument that aims to monitor the long-term trend of climate change. It is also vital for retrieving geophysical parameters that have small sensitivities to Tb changes including sea surface temperature. The warm calibration target should have uniform temperature distributions (both in-depth and planar) so that the monitored temperatures at limited positions can represent the effective temperature. The RFI problem in the C-band channels may be a difficult issue to solve. RFI signatures are most pronounced over the North America, Japan, and some part of the Europe. This mainly affects in retrieving soil moisture content. Any considerations to this problem are expected including shifting the center frequency or devise some mitigation techniques. Regarding the oxygen band channels around 60-GHz frequency, adding one or two sub-bands are desirable to measure atmospheric temperature profile in the troposphere and are still being discussed. In designing the AMSR instrument, additional sub-bands were very interesting but abandoned due to indeterminable hardware restriction.

This AMSR follow-on instrument will also play an important role in forming the Global Precipitation Mission (GPM) constellation. An instrument performance including

characteristics of the channel set and the high-spatial resolution achieved by the large reflector will be suitable for precipitation retrieval.

Table 2.2.1. Major specifications of ADEOS-II AMSR instrument

Center Freq. (GHz)	Band Width (MHz)	3dB Beam Width (deg)	Ground IFOV Scan x along track (km)	NEΔT @150K (K)
6.925	350	1.8	40x70	0.34
10.65	100	1.2	27x46	0.7
18.7	200	0.65	14x25	0.7
23.8	400	0.75	17x29	0.6
36.5	1000	0.35	8x14	0.7
50.3	200	0.25	6x10	1.8
52.8	400	0.25	6x10	1.6
89.0A	3000	0.15	3x6	1.2
89.0B	3000	0.15	3x6	1.2

3. Sensor Synergism

3.1. Wind Retrieval under Rain

It has become clear in the Scatterometer Science community, that any future mission must be accompanied by an AMSR or equivalent sensor that provides atmospheric measurements and suitable data products. The AMSR and its predecessor, the TRMM-TMI have demonstrated that they can produce a large number of atmospheric and sea surface data products. While substantial advances in oceanography and meteorology have been made, some important studies have been impeded by the presence of rain-contaminated wind vector estimates in the QuikSCAT and the ADEOS-II/SeaWinds data products. When rain-flagged wind observations data is omitted, low pressure systems are systematically flagged out, which has a serious impact on estimates of ocean circulation and climatic studies. For example, the results obtained during studies of high-wavenumber, surface wind forcing, have been shown to contain significant biases and discrepancies (Milliff et al., 2004; Chelton, 2004). Similar problems occur in a wide range of user applications. Comparisons of scatterometer wind magnitudes with buoy winds indicate that the atmospheric rain contributions can create erroneously large wind estimates, depending on the rain rate and true wind (Weissman et al., 2002). These studies document the problems associated with the acceptance or rejection of erroneous data, during the analysis of small scale wind features and wind stress curl. It is widely accepted that the status-quo (using rain flags and statistical factors in the PO.DAAC products) is unsatisfactory, and that improved, rain-corrected winds are necessary for the oceanographic community in the future. What makes this problem so challenging is the very wide possible range of the multiple variables: wind speed, rain spatial distribution, overall intensity and surface rain rate. In addition, the relative distribution of stratiform versus convective rain rates needs to be estimated. Therefore only a very advanced sensor, such as AMSR, can provide the needed resources for improving the scatterometer performance in rain. The rapid temporal changes in the atmospheric precipitation distribution require the continuous support of the AMSR data co-mounted on the same observation platform.

The ADEOS-II mission enabled us, for the first time, to collect collocated and simultaneous radiometer and scatterometer measurements. This has provided a unique opportunity to study and better understand how rain modifies the scatterometer signal and impacts its wind estimates. Unfortunately, the abbreviated ADEOS-II mission did not provide a sufficiently long data set for many studies; nevertheless, various research activities are being pursued. In the process, we hope to learn what the relative importance is of the different components of the rain interference (e.g., the impact of attenuation, versus that of rain volume backscatter, versus that of the rain-induced surface roughening). Inclusion of the rain-induced surface roughening appears to be necessary (Draper and Long 2004a) but its proper parameterization is quite challenging. Rain striking the surface of the water causes rings, stalks, and waves from which the signal additionally scatters. The interaction of rain with the surface of the water also alters the wind-induced capillary wave field, further changing the backscatter directional dependence. Current research activities, by several groups of investigators, are vigorously

addressing all these problems. The presence of precipitation converts the Scatterometer measurement from that of only a wind speed and direction estimate within each wind vector cell, to that of a multivariable problem in an inhomogeneous volume.

We note that a SeaWinds or future scatterometer also provides information necessary for accurate SST retrievals, which the AMSR can make on a continuous basis. Wind direction must be known to obtain accurate SST retrievals for wind speeds greater than 5 m/s. Assuming the wrong wind direction or ignoring the wind direction dependence can result in errors in SST retrieval as large as 4 deg at 15 m/s.

Radiometers also may be able to provide a key piece of information for improving scatterometer wind observations: information about the boundary layer stability. This information is valuable to improving our understanding of the relationship between the scatterometer observation and near-surface wind and wind stress values.

The very strong rain signature in the scatterometer-measured normalized radar cross section, for both polarizations, can be shown to estimate the surface rain rate (Weissman et al., 2003). This is an indicator of the larger potential for in-depth studies of the combined utilization of AMSR and a next generation scatterometer.

Draper and Long (2004a) evaluated the effect of rain on SeaWinds measurements, finding that for some combinations of rain rate and wind, rain had little effect on the estimated wind, while for other combinations (particularly at high rain rates), the rain-contaminated wind estimates have severe errors. These are evident in the frequently observed "squaring-off" of SeaWinds wind estimates in hurricanes. For this reason, a rain-flag is required to indicate wind estimates are rain contaminated. Rain flagged winds are considered suspect. Until recently (see below), independent measurements were the only method capable of flagging SeaWinds measurements that are corrupted by rain. As demonstrated by the ADEOS-II/SeaWinds mission, AMSR is ideally suited for this purpose. AMSR has proven invaluable for accurately rain flagging SeaWinds data. It provides the precisely temporally and spatially collocated measurements required to accurate flag SeaWinds data.

Recently, a simple model for the backscatter from the ocean during rain was developed and validated with the aid of collocated data from the precipitation radar (PR) on board the Tropical Rainfall Measuring Mission (TRMM) satellite and SeaWinds on QuikSCAT (Draper and Long, 2004a). The model is based on using PR reflectivities and path-integrated attenuation values to determine the backscatter and attenuation from falling rain droplets averaged over the SeaWinds footprint. The enhancement in backscatter from rain interacting with the ocean surface is solved for with the aid of numerical weather prediction model winds and observed SeaWinds backscatter. The simple model estimates 95% of the observed rain-contaminated SeaWinds backscatter values to within 3 dB (Draper and Long, 2004a).

The new model provides a quantitative tool for assessing precisely when the wind is contaminated by rain (Draper and Long, 2004a), though further work is required to make

this technique operational. Although rain corrupts scatterometer winds, the sensitivity to rain can enable SeaWinds to also estimate the rain rate. A new simultaneous wind/rain estimation technique has recently been developed that is based on this model (Draper and Long, 2004b; 2004c). This algorithm is effective in identifying rain-contaminated winds. Careful comparisons of SeaWinds-derived and AMSR-derived rain estimates show that rain flags from the two sensors agree more than 90% of the time. (This validates both simultaneous wind/rain retrieval rain flagging and the independent AMSR-derived rain flags.) However, the real value of simultaneous wind/rain retrieval is that it can be used for correcting rain-contaminated wind estimates, i.e., it results in improved the accuracy of estimated winds. Draper and Long (2004b) showed that this is particularly true when AMSR rain estimates are available since AMSR-derived rain rates can potentially reduce the variance of the wind correction. Thus, in addition to providing a critical rain flag, AMSR measurements can be used to improve the accuracy of SeaWinds wind measurements in the presence of rain.

3.2. Complementary Wind Retrieval

Both AMSR and SeaWinds can measure ocean surface winds, but their measuring techniques are different. The technique for the former sensor is based on detecting a change of the microwave emission of the ocean surface induced by winds, and the one for the latter sensor is based on a backscatter of the microwave returned from the ocean surface. Comparison of ocean winds retrieved from AMSR and SeaWinds reveals that two winds are different in a range of strong wind speeds such as more than 15m/s. Even though this difference is small as an order of a few m/s, a mechanism of inducing the difference is unknown. This means that both two sensors are necessary for observing ocean winds with a deeply scientific level.

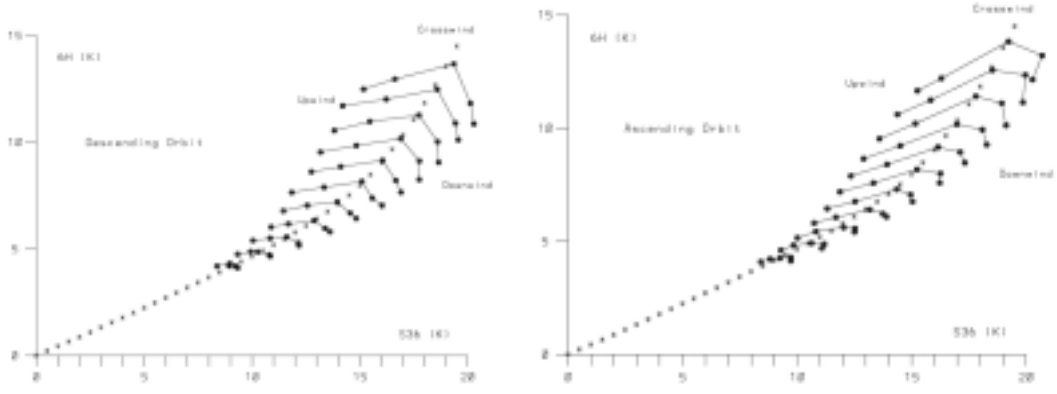

Figure 3.2.1. S36 (K) versus 6H (K) for descending (left) and ascending (right) orbits.

An example indicating that two winds are different is shown in Fig.3.2.1, where the left panel is for a descending orbit of ADEOS-II, and right one for an ascending one. The vertical axis of both figures is a 6GHz horizontal polarization (6H) related with ocean wind (unit; Kelvin), and the horizontal one is a 36GHz quantity (S36) related with ocean wind (unit; Kelvin). In both figures, a point of (S36, 6H) with the same SeaWinds wind speed is shown for several relative wind directions determined from SeaWinds wind direction and AMSR viewing direction. SeaWinds wind speeds are shown from 7 to 17 m/s with 1m/s interval, and relative wind directions from upwind to downwind with 45 degrees interval. Observation areas are limited to those southern less than 30S to avoid sun-glitter, and observation period is 10 days in April 2003. Comparison points are limited to one–third of observation swath in the left hand. Figures show that 6H or S36 are different between descending and ascending orbits, even though the same wind speed and relative wind direction. A possible explanation of this difference is that ocean winds are different in the eastern and western parts of cyclones, but further investigations are necessary.

4. Science Synergism

4.1. Water Cycle

The Water-Energy Cycle has been one of the scientific focus of NASA. It is one of the scientific priorities of the U.S. Climate Change Science Program (CCSP) and a main component of the international Global Energy and Water Experiment (GEWEX), Climate Variability and Predictability (CLIVAR) and Climate and the Cryosphere (CliC) research programs.

The natural law on the conservation of mass governs the hydrologic balance in the atmosphere. The temporal change in water storage and the divergence of the moisture transport integrated over the depth of the atmosphere Θ has to balance the fresh water flux at the surface. The fresh water flux at the surface is the difference between evaporation (E) and precipitation (P). The temporal change of water storage can only be transient, and, when averaged over time, the balance is between $\nabla \cdot \Theta$ and E-P. Monitoring these two terms is critical to the characterization of the hydrological cycle and climate change. Direct in situ measurements of Θ, E, and P are extremely sparse over ocean. While microwave radiometers, such as AMSR, can be used to estimate E and P, the estimation of Θ requires additional dynamic parameters, which must comes from the scatterometer.

Spacebased microwave radiometers, such as AMSR, have provided estimation of P over oceans for many years. Liu and Niiler (1994) pioneered a method for estimation of E using radiometer data, and subsequent improvements were reviewed by Liu and Katsaros (2001). The method to estimate Θ, using a combination spacebased radiometer and scatterometer was recently demonstrated by Liu and Tang (2005). The three terms were estimated independently, using QuikSCAT and TMI, by Xie and Liu (2005). The similar geographical distributions of $\nabla \cdot \Theta$ and E-P as shown in the Figure 4.1.1, is one of the best validation of the estimation techniques and a clear demonstration of the science synergism of the two instruments. Xie and Liu (2005) also show that $\nabla \cdot \Theta$ and E-P agree from intraseason to interannual time scales and both terms show strong lag coherence with surface salinity at selected tropical locations. The combination of microwave radiometer, (e.g., AMSR), and scatterometer (e.g., SeaWinds) is very important to the characterization, understanding, and prediction of the hydrologic-energy cycle.

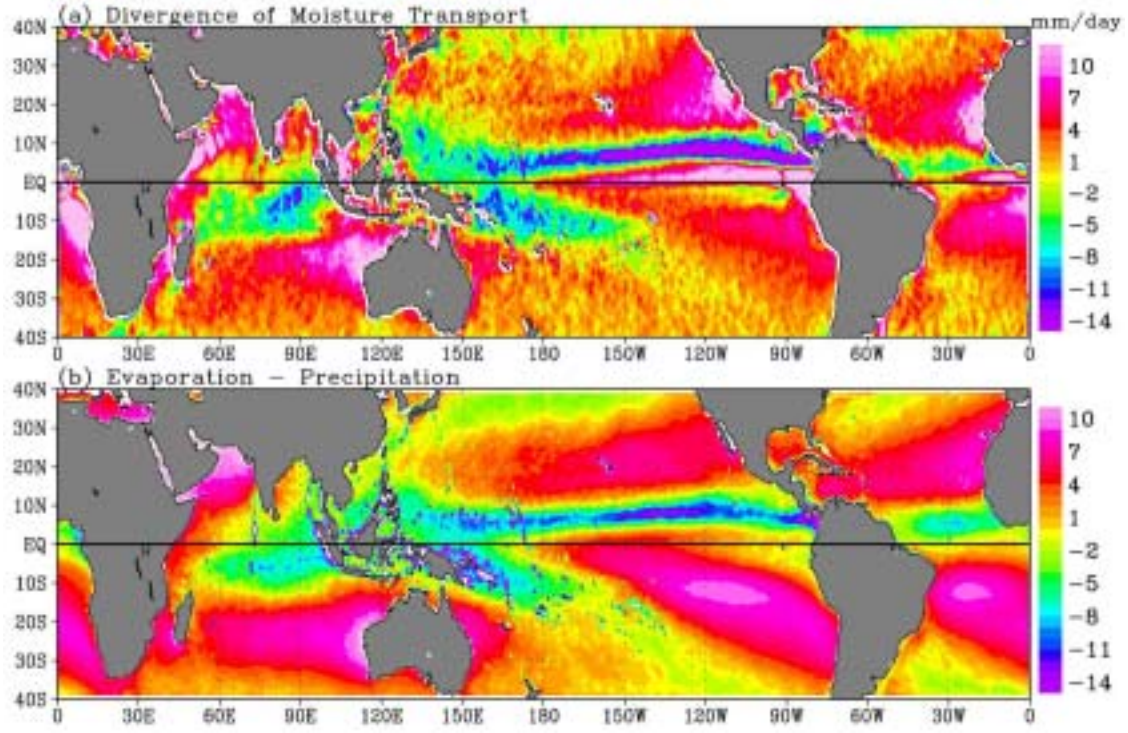

Figure 4.1.1. Annual mean (a) divergence of moisture transport integrated over the depth of the atmosphere, and (b) evaporation-precipitation. Evaporation and precipitation were estimated independently from TRMM data. Moisture transport was estimated from a combination of TRMM and QuikSCAT data. From Xie and Liu (2005)

4.2. Monsoon

Monsoon is the seasonal change of winds. The change is caused by the reversal of land-ocean temperature gradient. The oceanic influence is manifested through continental rain. Monsoons affect an extensive area of the world with large population. Their annual onset, intensity, and retreat vary greatly, and the variation has strong economic impact and may cause severe human suffering.

To study oceanic influence on the precipitation in India, Θ estimated based on the method described by Liu and Tang (2005), using data from TMI and SeaWinds, was interpolated to the coastline the Indian subcontinent and the component normal to the coastline was computed and related the precipitation over land. Figure 4.2.1, from Liu and Tang (2004), shows that, during the summer monsoon, from May to November, moisture is transported into India from the Arabian Sea (green curve in Fig. 4.2.1b) and transported out to the Bay of Bengal (red curve in Fig. 4.2.1b). The transport is reversed for the rest of the year,

with low activity in all segments between February and May, as expected. The total moisture advected from the near-by oceans (black curve in Fig. 4.2.1a) is in phase with the total rainfall integrated over land (blue curve in Fig. 4.2.1a). During the peaks of summer monsoon, the moisture from the ocean exceeds the precipitation, suggesting that moisture may move north over land.

The transport out of the eastern coastline, however, occurs earlier than the transport in from the western coastal line, as shown in Figure 4.2.1d. The delays are particular sharp and long in 2002 and 2003. There were suggestions that the onset of summer monsoon occurs earlier in the Bay of Bengal than in the Arabian Sea, and these results are the clearest and most direct observations. This delay may cause droughts in India just before the onset of the summer monsoon. The synergism of the active and passive microwave sensors again allow us to study an important natural process that has strong impact of human well being.

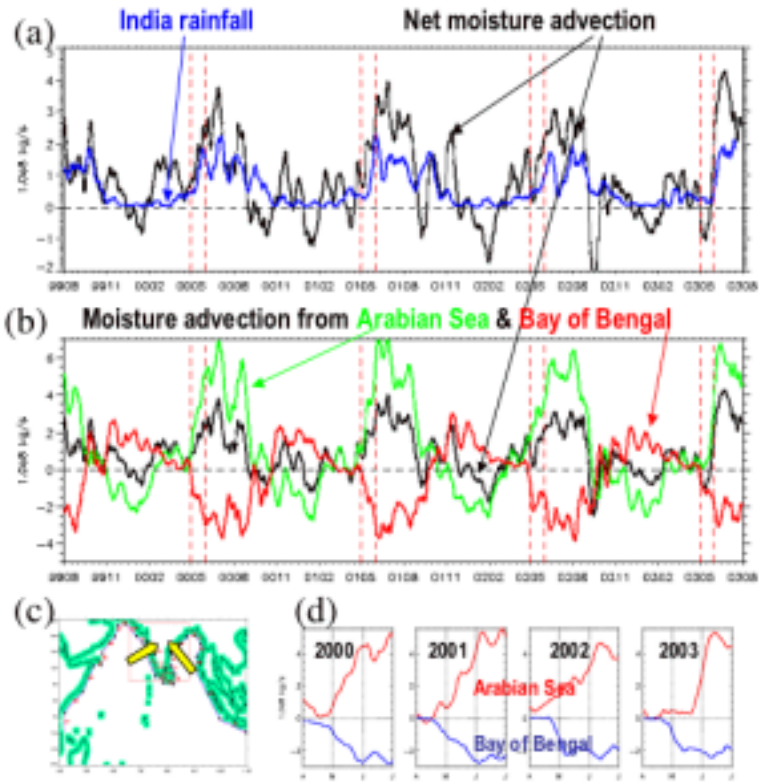

Figure 4.2.1. Time series of (a) rainfall integrated over the Indian subcontinent (blue) compared with net moisture advected from the surrounding ocean (black), (b)moisture advection from the Arabian Sea (green), from the Bay of Bengal (red), and the total (black), (c)map of the area, and (d) expanded time series of moisture advection during summer onsets for four years. From Liu and Tang (2004).

4.3. Tropical Cyclones

In situ observations over the ocean are extremely sparse during a tropical cyclone and conventional satellite data only provide cloud imagery at the top of the storm. Tropical cyclones are devastating when they are accompanied by strong winds and heavy rain. The combination of spacebased microwave radiometer and scatterometer provided the opportunity to observe both wind and rain in tropical cyclones before landfall. The coincident measurements of surface wind and rain reveal the interplay between the dynamics and the hydrologic balances of the storms. When applied to Hurricane Floyd, Liu et al. (2000) shows that the high spatial resolution of ocean surface winds measured by QuikSCAT improves the computation of the moisture transport, the vertical profiles of moisture sink and diabatic heating and E-P at the surface. The results were validated using observations of surface rain and rain profiles by the microwave radiometer and radar on TRMM. The close relationship between the dynamic and hydrologic parameters is visible in Fig. 4.3.1 as hurricane Floyd approaches the Bahamas on September 12, 1999.

The landfall of a tropical cyclone may devastate the economy and cause human lives. Yet a tropical cyclone may also enhance other form of life – the primary productivity in the ocean. Ocean productivity affects not only the local fishery, but also the uptake of carbon dioxide, an important greenhouse gas, and a major cause of natural and man-made climate changes. Documenting the thermal and biological responses to the passages of typhoons using ships with prescribed tracks, or using moored buoys with fixed locations, is difficult because of the transient and severe nature of the typhoons. Two spaceborne microwave sensors, QuikSCAT and TMI, allow us to measure ocean surface wind vectors and sea surface temperature under cloud cover of typhoons, day and night. QuikSCAT observed typhoon Kai-Tak lingering for several days in the northern part of South China Sea between 5th and 8th July 2000. There is a sharp increase of Ekman pumping velocity (the vertical velocity resulted from wind induced surface convergence and uplifting of the thermocline) computed from QuikSCAT winds, during the passage of Kai-Tak (Fig. 4.3.2a). The sea surface temperature dropped from 30°C before the typhoon to 22°C the day after the typhoon departure, a drastic 8°C drop as revealed by TMI in Fig. 4.3.2b. Lin et al (2003) observed 300 time increases in chlorophyll-a (indicating biological activities) within a few days using observations by the Sea Viewing Wide-Field-of-View Sensor (SeaWifs).

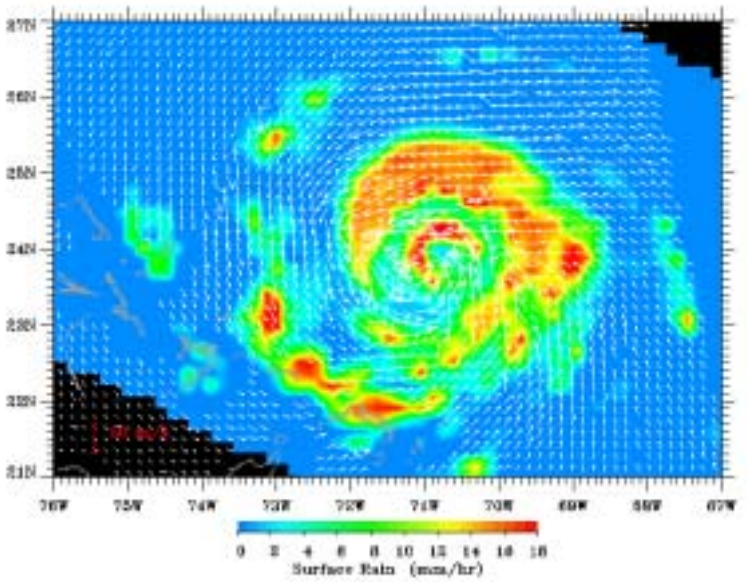

Figure 4.3.1. Hurricane Floyd is revealed by wind vectors (white arrows) from SeaWinds and surface precipitation (color image) from the microwave imager, on September 12, 1999, along the ground-tracks of QuikSCAT and TRMM. From Liu et al. (2000).

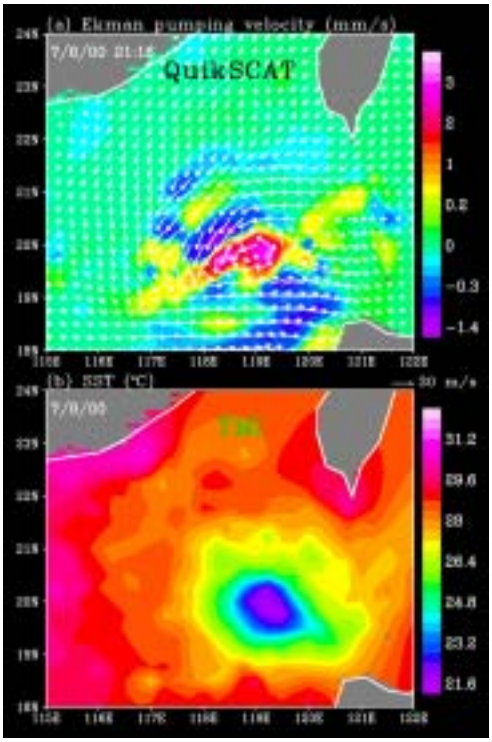

Figure 4.3.2. The effects of Typhoon Kai-Tak as, (a) wind vector (white arrows) superimposed on the color image of Ekman pumping velocity on July 8, 2000, and (b) sea surface temperature observed by TMI on July 9, 2000.

4.4. Ocean-Atmosphere Coupling

The vast ocean is poorly sampled by traditional ship-based observations. Cloud-penetrating, space-based microwave remote sensing is revolutionizing ocean observation, revealing new phenomena by its unprecedented sampling and resolution. The combined microwave radiometer and scatterometer observations and analysis are particularly powerful since sea surface temperature (SST), surface wind, and cloud liquid water are strongly coupled and their interaction is an important yet poorly observed process shaping Earth climate. The following are two examples of recent combined analysis of QuikSCAT scatterometer and Tropical Rain Measuring Mission (TRMM) microwave imager (TMI) observations that has led to surprising discoveries.

Longest wake on Earth. The northeast trade winds prevail over the subtropical North Pacific. As these trades impinge on the tall mountains of Hawaii, a pair of wind vortices is generated on the lee. The first 6-month QuikSCAT data reveals that this island wake persists for an unusually long distance of 1000s km, which TMI and historical data shows is due to a close interaction of the ocean and atmosphere triggered by the island-induced wind vortices (Fig. 4.4.1). Indeed, surface winds are converging onto the warm water band west of Hawaii, as captured by QuikSCAT and TMI. It is amazing that tiny islands of Hawaii can cast such a long shadow on much of the vast North Pacific Ocean.

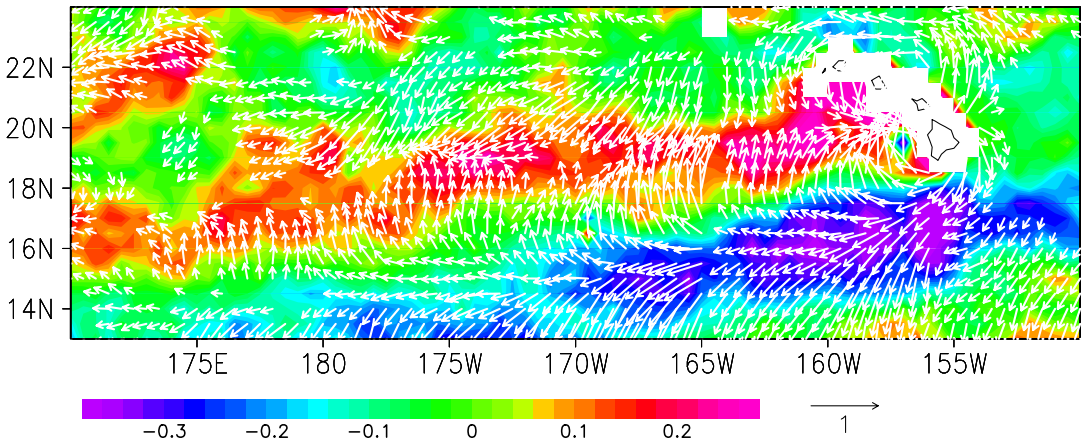

Figure 4.4.1. SST (color in °C) and wind (m/s) variations induced by orographic effect of Hawaii. Basin-scale background fields as represented by 8° meridional running-means have been removed. From Xie et al. (2001).

Bathymetric effect on wind. It may sound improbable that submerged ocean bottom topography can change winds and clouds, but satellite observations reveal such a bathymetric effect over the Yellow and East China Seas. Most of these seas are shallower than 100 m. In winter the northerly monsoon blows the frigid and dry continental air over the seas, generating warm and cold tongues over deep channels and shallow bank, respectively. QuikSCAT and TRMM measurements reveal remarkable spatial co-variations in wind and cloud with SST. Convergent wind and increased cloudiness are found over the bathymetric-induced warm tongues. In particular, one such band of co-variation between ocean and atmosphere meanders through the Yellow Sea between China and Korea for an amazing distance of 1000 km, following a deep channel that was an ice-age river (Fig. 4.4.2).

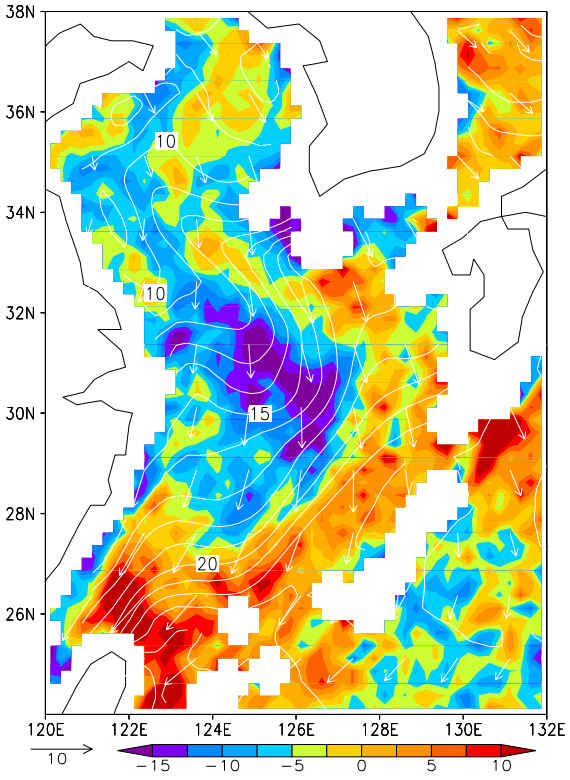

Figure 4.4.2. TMI SST for January-March 2000-02 (contours in ^{o}C) over the Yellow and East China Seas, along with QuikSCAT wind velocity (vectors in ms^{-1}) and divergence (color in 10^{-6} s^{-1}). From Xie et al. (2002).

4.5. Tropical Climate

The studies provided by SeaWinds program have demonstrated the importance of combined observations between AMSR and Scatterometer in understanding and monitoring the climate variabilities of tropical convection, the intertropical convergence zone (ITCZ) and El Nino/Southern Oscillation (ENSO). This is because ENSO and climate variability of the ITCZ are determined by atmosphere-ocean interaction at the ocean surface, especially within the regions of convective/rainfall centers.

For example, only all-weather observations of ocean surface winds such as those of QuikSCAT can adequately observe and monitor climate variability of Walker and Hadley circulations (Pan et al., 2001). All-weather ocean surface winds also allow us to more clearly capture the ITCZs. As shown by Liu and Xie (2002), the double ITCZ in the eastern Pacific cold tongue and in Atlantic is much stronger than previously anticipated. Because of frequent present of drizzles in these regions, WINDSAT cannot adequately detect surface wind in this region. In the western Pacific warm pool region where rainfall presents frequently, Yu et al. (2001) are able to show that the westerly wind anomalies are associated with cold surge from Asia during ENSO using the QuikSCAT observations. Given the importance of ocean surface winds on the cold water upwelling and consequently SSTs in the eastern Pacific cold tongue, and the role of westerly anomalies in initiating ENSO, the capability of scatterometer demonstrated in their studies is important to provide accurate surface winds needed for a better understanding and prediction of ENSO. Indeed, Chen et al. (1999) and Chen (2003) have shown that use of QuikSCAT ocean surface winds as an initialize condition can drastically improve the ENSO prediction.

The climate variability of Atlantic ITCZ has received increasing attention from the U.S. climate research community and strong endorsement of US CLIVAR (Climate Variability and Predictability) program. One of the priority questions is to understand the interaction between the cross-equatorial SST gradient and the migration and intensity of the Atlantic ITCZ. The interannual and decadal changes of the latter strongly influence the frequency and locations of the tropical storms over Atlantic, as well as monsoon over NE Brazil and western Africa (e.g., Nicholsen and Entekhabi 1986; Ropelewski and Halpert 1987). Conventional wisdom believes that such variabilities are dominated by the influences from ENSO and the North Atlantic Oscillation (NAO) (e.g., Covey and Hastenrath 1978; Hansen and Bezdek 1996). However, recent studies show that these two forcings only explain a half of the observed interannual and decadal variations of the ITCZ (e.g., Liu et al., 2004). The remaining climate variabilities are determined either by interaction between ITCZ and underlying SSTs gradient (e.g., Xie and Tanimoto, 1998; Chang et al., 2000; Liu et al., 2004), or possibly by other forcings (Biasutti et al., 2003; Ruiz-Barradas et al. 2003). Among other forcings, the potential influence from continental convection is recognized (Science plan of Atlantic Maritime ITCZ, 2004). But observational evidence was previously absent and numerical models have given controversial answers to this question.

Fu et al. (2004) have demonstrated the unique role of scatterometer and AMSR measurements in further understanding of the Atlantic ITCZ climate variabilities. Because the AMSR and scatterometer board on QuikSCAT can provide a sufficiently accurate retrieval of twice daily ocean surface winds, especially under rainy conditions for several years. Such observations allow us to detect changes of ocean surface winds before and after the strong episodes of South American rainfall, as shown in Fig. 4.5.1. The observed diurnal variations of the ocean surface wind anomalies peak in late afternoon as continental rainfall peaks (Fig. 4.5.2). This further suggests that such wind responses are not forced by oceanic processes. Using wind stress derived from QuikSCAT, along with surface turbulent and radiative fluxes derived from ECMWF (European Centre for Medium-Range Weather Forecasts) reanalysis to force an ocean mixing layer model, Fu et al. (2004) have found that the ocean surface winds changes induced by continental rainfall can in some years induced SST anomalies comparable to those of ENSO.

Currently, the length of SeaWinds ocean surface wind observation has begun to allow scientists to examine the interannual variations of ITCZ, but QuikSCAT has exceeded its expected lifetime by years. A continuation of coinciding scatterometer and AMSR observations will play a crucial and irreplaceable role in studying interannual to decadal variations of ITCZ and tropical convection, including the influence of ENSO and NAO.

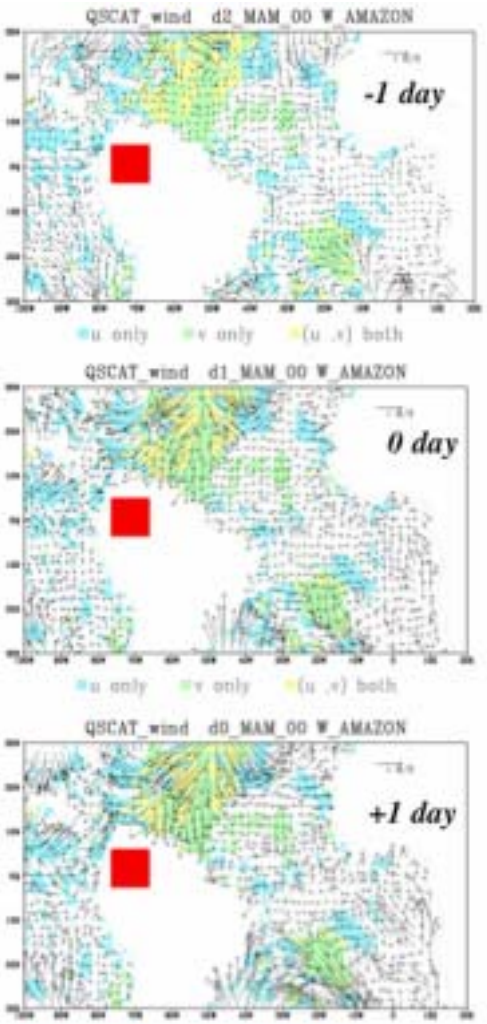

Figure 4.5.1. Composite daily changes of ocean surface winds from the previous day at 7-8 pm local time for the strongest 20% of the rainy events over the western Amazon region (indicated by the red box) for the March-May season during the period of 2000-2003. Top panel: 1 day before the peak rainy events; Middle panel: The day of peak rainy events; Bottom panel: 1 day after the peak rainy events. Winds (vector) are derived from QuikSCAT and rainfall from TRMM daily rain rate. The color shades indicate that the areas where winds changes are statistics significant with 95% confidence based on Monte-Carolo test for 1000 realizations at each grid.

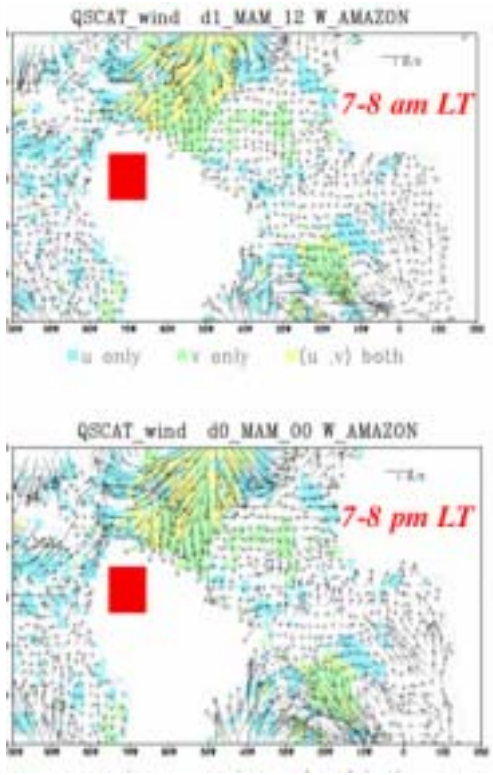

Figure 4.5.2. As in Figure 1 but for 7-8 am local time (Top panel); Bottom panel: 7-8 pm local time, 1 day after the peak rainy events.

4.6. Ocean's Response to Wind and Hydrologic Forcing

Climate variability has a huge amount of impacts to the society. Climate state is driven by the interactions among atmosphere, ocean and land. The interaction of the atmosphere and ocean, as one interaction in the climate variability, has a wide range of time scales from second to century (or more). The interaction has also an important effect on hydrological water cycle. The water cycle has the recent most important issue in the world. It is not only an environmental problem but also human existence and security issues. For solving these issues, developments of real-time monitoring and forecasting systems are crucial. Ocean model, as well as atmospheric and land models, constitutes the systems. The ocean model is driven by the momentum, heat and fresh water fluxes.

Recent developments of the numerical weather prediction (NWP) in the atmosphere give the fluxes as its output for ocean modeling. Many oceanographers have been adopted the NWP outputs as the forcing. However, if we examine the model results, we understand that the resolution and accuracy of the NWP products are considerably shortage. Also the spatial resolution of the NWP product is not enough for understanding ocean's response to wind and hydrologic forcing. Figure 4.6.1 shows an example of wind fields of QuikSCAT/SeaWinds and National Oceanic and Atmospheric Administration/National Centers for Environmental Prediction (NOAA/NCEP) NWP products in April 1st, 2003. We can recognize the shortage of NWP wind fields from this figure. Moreover, wind speed is an important factor for estimation of evaporation (latent heat flux) over the sea surface. Figure 4.6.2(a) shows a wind field of QuikSCAT in January 2000. We can find significant features of the ocean surface wind field in the coastal region related to orographic effects. On the other hand, we cannot find significant features related to this wind field for (b) latent (evaporation) and (c) sensible heat flux fields provided by ERA40. This is due to the broad spatial scale of (d) the ERA40 wind field. The ocean has a typical spatial scale (which is called baroclinic Rossby's radius of deformation), which is 10-100km in the region of Figs. 4.6.1 and 4.6.2. For the realistic ocean modeling and forecasting of climate, the forcing fields that resolve the scale of the baroclinic Rossby's radius of deformation are crucial. In order to produce the fields, only satellite (microwave scatterometer and radiometer) can provide the information.

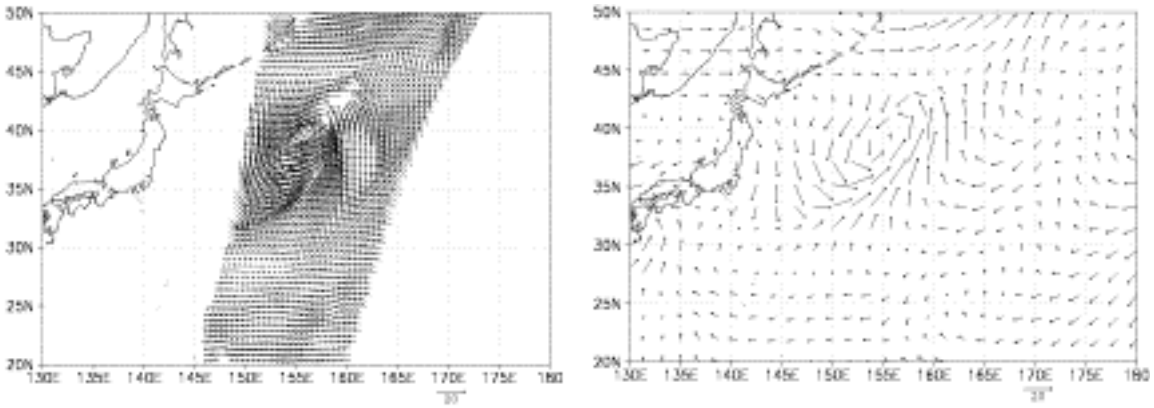

Figure 4.6.1. Wind fields from QuikSCAT/SeaWinds (left), and the NCEP NWP product (right).

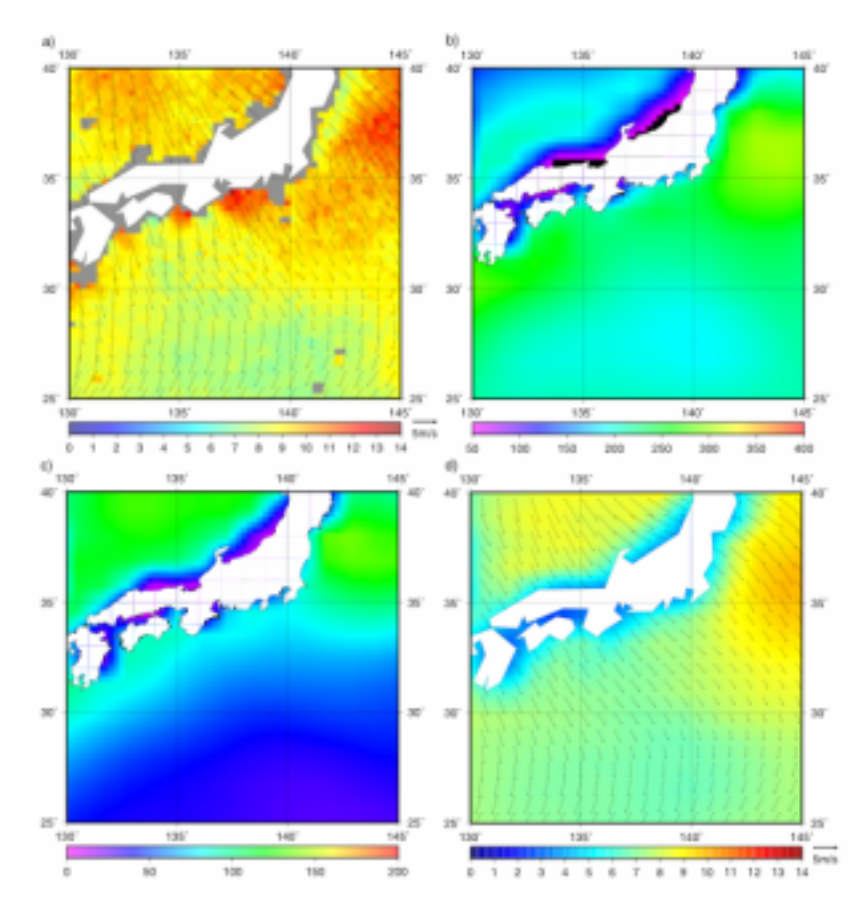

Figure 4.6.2. (a) QuikSCAT wind field, (b) ERA40 latent heat flux (evaporation) field, (c) ERA40 sensible heat flux field, and (d) ERA40 wind field, in January 2000.

4.7. Operational Numerical Weather Prediction

Recently microwave radiometer data have been used in operational numerical weather prediction (NWP) centers to improve very short-range to medium range forecast including tropical cyclone tracking. For example, Japan Meteorological Agency (JMA) has used precipitable water and rain rate derived from the Special Sensor Microwave/ Imager (SSM/I) and the Tropical Rainfall Measuring Mission (TRMM) Microwave Imager (TMI) data in the operational meso-scale NWP model since 15 October 2003. These data improve precipitation distribution and the intensity for very short-range forecast up to 18 hours. To extend the data coverage precipitable water and rain rate from the Advanced Microwave Scanning Radiometer for Earth Observing System (AMSR-E) aboard the NASA's Aqua satellite data have been also used in the meso-scale model since November 2004.

Microwave scatterometer data has been also used in operational NWP centers to improve the forecasts especially for position of frontal zone and tropical cyclone center over the last 10 years. For example, JMA uses sea surface wind derived from SeaWinds on QuikSCAT in the operational meso-scale NWP model as well as the operational global NWP model as of November 2004. Though the data are essential to identify circulation and convergence related to atmospheric disturbance over ocean, it is often noted that sea surface wind retrieval from scatterometer is of less quality in heavy rain area where is the key area to improve forecast.

Two benefits of the synergy use of a microwave radiometer and a microwave scatterometer aboard in a satellite should be pointed out for the NWP application. Firstly, high-quality surface wind data, precipitable water and rain rate data are available because the surface wind retrieval with the scatterometer takes in rain correction by the radiometer and the water vapor and rain retrieval with a radiometer takes in wind direction correction by the scatterometer. Secondly, it is convenient for NWP application to have sea surface wind, water vapor and rain data simultaneously because the relationships between wind and the hydrological parameters are analyzed without considering observation time lag. Figure 4.7.1 shows the near simultaneous observation well depicts a correspondence between strong convergence related to front and tropical cyclone and heavy rain bands.

Definitely a scatterometer much improves the operational NWP application as well as a microwave radiometer does. Furthermore the benefits are magnified synergically when the two instruments are aboard a satellite together.

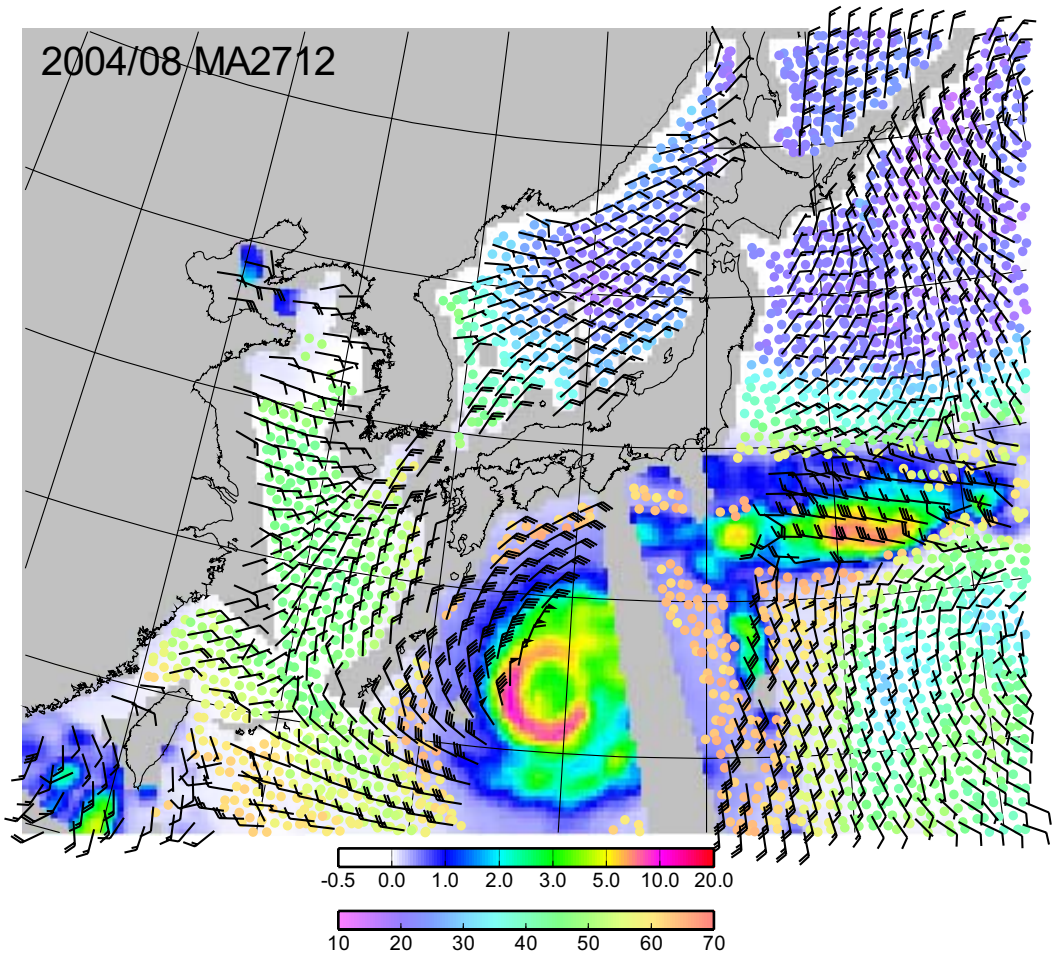

Figure 4.7.1. Surface wind derived from QuikSCAT/SeaWinds and precipitable water (colored circle dots) and rain rate (colored square dots) derived from SSM/I and TMI. All plotted data are used in the JMA meso-scale NWP model. The observation time ranges between 09-15UTC 27 August 2004.

4.8. Cryospheric Studies

Sea ice and its snow cover. Over the past 30 years the Arctic sea ice cover has been retreating and this retreat has accelerated over the past few decades as shown from an analysis of satellite microwave radiometer data (Cavalieri et al., 2003). During the last few years there has been a significant reduction in the perennial (multiyear) ice cover in the Beaufort Sea during freeze-up and a reduction of seasonal (first-year) ice in the East Arctic (Nghiem, 2004). Some studies predict the disappearance of the perennial ice cover within the next century (Comiso, 2002). Furthermore, analyses of submarine data reveal significant changes in the thickness of the perennial ice cover across the Arctic (Rothrock et al., 1999; Holloway and Sou, 2002). The rate of sea ice thinning is dependent on several factors including the depth of its snow cover which insulates the ice from the cold winter air limiting its growth during winter. Whether the observed changes in the Arctic result from global warming or are more the result of natural climate variability remains to be determined. Nonetheless, it is essential that sea ice concentration, sea ice snow depth, and ice thickness continued to be monitored and studied to understand the causes of the observed sea ice variability.

The most successful tool in studying sea ice variability is the spaceborne microwave radiometer. Data sets based on these sensors have been developed and span three decades (Cavalieri et al., 2003). While the microwave radiometer provides the best measure of the global sea ice cover (extent and concentration), the scatterometer has been shown to be more useful for distinguishing between seasonal (first-year) and perennial (multiyear) ice types (e.g., Gohin and Cavanie, 1994; Gohin, 1995; Gohin et al., 1998).

Recent work has shown that there was a “surge” of old perennial ice from the Beaufort gyre to Fram Strait in 1988 through 1990 decreasing the fraction of thick, ridged ice within the central Arctic (Pfirman et al., 2004). A series of studies using NSCAT data from ADEOS and QuikSCAT data show that scatterometers provide excellent mapping of sea ice drift (Liu et al., 1998, 1999) and compare very well with SSM/I data (Zhao et al., 2002).

New techniques have been developed using QuikSCAT/SeaWinds and satellite microwave radiometer data to estimate the onset of melt and the rate of sea ice decay (Howell et al., 2004; Anderson and Drobot, 2001). This is of particular importance, because differences in ice thickness between consecutive winters are highly correlated with the length of the melt season (Laxon et al., 2003). The growth and decay of sea ice is modulated by its snow cover. A comparison of AMSR-E snow depth measurements on sea ice with surface-based measurements seems to indicate a dependency of the snow depth retrieval on surface roughness something that a scatterometer can be used to measure and thus correct (Markus et al., 2004). The synergism of using spatially and temporally coincident radiometer and scatterometer measurements will allow us to more effectively measure the sea ice mass balance of the Arctic Ocean.

Snow water equivalent on land. Snow cover and snow water equivalent on the Earth's surface are a major storage component of the global hydrological cycle. Snow is the most annually variable part of this storage component covering approximately 50% of the continental northern hemisphere in mid winter to almost 0% coverage in mid summer. This northern hemisphere coverage represents about 98% of global seasonal snow cover extent (SCE) (Armstrong and Brodzik, 2001). According to Brown (2000), ground observations from mid-latitude stations for 1915-1997 have shown a decrease in snow cover extent by approximately 3.1 x 10^6 km^2 $(100\ yr)^{-1}$ which represents approximately a 0.1% per year decrease. The satellite record from 1979 to 2000 shows a hemispheric decrease of 0.2 % per year in snow cover extent (Armstrong and Brodzik, 2001) suggesting an accelerated rate of reduction of hemispheric SCE in the latter part of the twentieth century. Accompanying the observed SCE reduction is a suggestion that there is a shortening of the snow season accompanied by an increase in snow accumulation during the contracted snow season. This increased accumulation, or snow water equivalent (SWE), was found by Brown (2000) but has not been independently verified either by direct satellite observations or by land surface model simulations.

Global snow cover also has an important influence on climate through its effect on the global water cycle and energy budgets at the surface and lower atmospheric levels. It has been shown that the timing of the onset and duration of the snow season can have associations with climate predictability (e.g., Cohen and Entekhabi, 1999). Also, studies have suggested that regional antecedent spring snow accumulations can modulate summer weather (Lo and Clark, 2002), and interannual snow cover extent variations have been linked to monsoon dynamics (Bamzai and Shukla, 1999). Studies such as these that combine snow data with global circulation models have highlighted weaknesses in the parameterization of snow in General Circulation Models (GCMs) for global climate simulations (e.g., Schlosser and Mocko, 2003) and demonstrate that consistent estimates of global regional SWE are important for realistic GCM simulations (Drusch et al., 2004)

Spaceborne passive microwave instruments have measured the interaction of natural upwelling microwaves from the Earth for over 30 years. The relationship between radio brightness temperature and SWE is well understood both from a theoretical modeling standpoint and from a practical retrieval perspective (Chang et al., 1987). The intensity of microwave radiation emitted through and from a snowpack depends on several geophysical properties: physical temperature, SWE, grain size, density, and underlying surface conditions of the snowpack, the vegetation cover character and the wavelength of observation. Several studies have shown the utility of satellite passive microwave estimates of SWE from dry seasonal snowpacks with some success. Globally, Kelly et al. (2003) have developed a dynamic algorithm based on radiative transfer modeling of Tsang et al. (2000) and Chang et al. (1987). Derksen et al. (2003) describe a regional approach to estimate SWE in western Canada using satellite passive microwave observations from the SSM/I. Recently, Grippa et al. (2004) have demonstrated a dynamic algorithm to estimate seasonal SWE in Siberia. Current efforts are focused on the use of data from AMSR-E since it has enhanced spatial resolutions at the frequencies of choice. Errors in SWE retrievals are known to be related to uncertainties about the geophysical parameters at the time of retrieval and attempts have been made to improve

SWE estimates through the constraint of snow grain size parameterization in the retrieval schema to improve the SWE estimates (e.g., Kelly et al. 2003). By accounting for the first order variables that directly affect SWE retrievals, especially grain size and forest cover, estimate uncertainties of SWE will continue to be reduced.

Sensor synergism exists potentially with QuikSCAT/SeaWinds observations. The onset of snowmelt has been detected effectively by Nghiem and Tsai (2001) using QuikSCAT data. This is of particular importance because AMSR-E and other satellite passive microwave sensors are not capable of directly detecting wet snow. Thus, there is a good synergy between the accumulation of snow from AMSR-E and the identification and monitoring of snowmelt from QuikSCAT. Furthermore, it has been shown that C-band and L-band radar responses from forest cover can be used to estimate timber volume of the forest (Baltzer et al., 2002). This information can be of great use for the passive retrievals of SWE. With the addition of the Moderate Resolution Imaging Spectroradiometer (MODIS) estimates to map, there is an excellent potential to map snow accumulation from the start of the snow season right through to the end of the melt phase. Both hydrologically and climatologically, this is a key ability to possess in order that a consistent data set of global snow accumulation can be monitored.

The assessment of errors in passive microwave SWE retrievals is not straightforward. Foster et al. (2005) recently has demonstrated a method to quantify the systematic errors from passive microwave retrievals. Chang et al. (2005) have proposed a method to estimate the non-systematic errors from passive microwave snow depth estimates over land. Together, these approaches should help facilitate the formal assimilation of passive microwave estimates of SWE in land surface models as demonstrated by Sun et al. (2004).

4.9. Land Applications

A number of Earth observation space missions have been flown with passive and active microwave sensors on board. These include Skylab, Seasat, TOPEX, Jason, TRMM, and ADEOS and ADEOS-II, among others. Although in general these sensors were not designed specifically for land applications, their data have been analyzed over land and have provided very useful information in characterizing passive and active land signatures and the temporal and spatial variability of surface soil moisture and vegetation cover. In particular, the wide-swath global coverage of SeaWinds and AMSR instruments on ADEOS-II spacecraft have provided the first opportunity to examine global land features on a frequent time-scale (approximately every two days or better) simultaneously with passive and active microwave sensors. Initial examinations of these combined data sets have indicated the complementary sensitivities of these sensors to soil moisture and vegetation, suggesting that processing of the data jointly could provide significantly enhanced benefits over each sensor alone.

Typically data from the ADEOS-II and earlier passive and active sensors have been analyzed independently, or combined at the geophysical levels. More recently, attention is being paid to combined analyses at the sensor data levels to optimally derive a common product such as soil moisture. Active and passive signatures of Earth surfaces indicate sensitivities to common features, through the dielectric and geometric properties of the surface and subsurface media, though the relative sensitivities of the radar and radiometer to these properties may be quite different. Hence the information content of the two techniques is complementary to varying degrees, depending on the wavelengths, polarizations, spatial resolutions and viewing geometries of the sensors. Optimal retrieval tools and techniques are under development to derive information from combined passive and active data sources, adapted to the specific geophysical phenomena being sensed. This includes joint electromagnetic characterization of radar backscatter and radiometric emission from media with surface or volume scattering, and heterogeneous layered surfaces (such as vegetation-covered soils); estimation techniques for joint retrieval of geophysical parameters from passive and active data, including effects of data noise and spatial resolution; validation studies using experimental observations; and illustrations of applications to specific geophysical problems such as soil moisture, freeze-thaw, and vegetation sensing, and flood monitoring.

The Hydros soil moisture and freeze-thaw mission, planned for launch in 2010, will carry passive and active L-band sensors specifically with the objective of enhanced soil moisture and freeze-thaw estimation. L-band sensors penetrate deeper into the vegetation, snow cover (if any), and soil, allowing more information on the moisture to be obtained at greater depths in the medium than at C-band and higher frequencies. In order to separate out the multiple contributing factors in the sensor signal, and to understand the moisture characteristics of different components of the vegetation and soil, it is important to measure the microwave properties at several wavelengths, with both passive and active sensors. Combining passive and active sensing at L-band (Hydros) with passive and active sensing at C- and K-band sensors, would provide an optimum approach to characterizing the hydrologic properties of the land surface.

5. References

Anderson, M. R, and S. D. Drobot, Spatial and temporal variability in snowmelt onset over Arctic sea ice. *Annals of Glaciology*, **33**, 74-78, 2001.

Armstrong, R.L., and M.J. Brodzik, Recent northern hemisphere snow extent: a comparison of data derived from visible and microwave satellite sensors. *Geophysical Research Letters*, **28**, 3673-3676, 2001.

Bamzai, A.S., and J. Shukla, Relation between Eurasian snow cover, snow depth and the Indian summer monsoon: an observational study. *Journal of Climate*, **12**, 3117-3132, 1999.

Baltzer, H., J.R. Baker, M. Hallikainen, and E. Tomppo, Retrieval of timber volume and snow water equivalent over a Finnish boreal forest from airborne polarimetric synthetic aperture radar. *International Journal of Remote Sensing*, **23**, 3185-3208, 2002.

Brown, R., Northern hemisphere snow cover variability and climate change, 1915-1997. *Journal of Climate*, **13**, 2339-2355, 2000.

Cavalieri, D. J., C. L. Parkinson, and K. Ya. Vinnikov, 30-Year satellite record reveals contrasting Arctic and Antarctic decadal sea ice variability. *Geophysical Research Letters*, **30**(18), 1970, doi:10.1029/2003GL018031, 2003.

Chang, A.T.C., J.L. Foster, and D.K. Hall, Nimbus-7 derived global snow cover parameters. *Annals of Glaciology*, **9**, 39-44. 1987.

Chang, A.T.C., R.E.J. Kelly, E.J. Josberger, R.L. Armstrong, J.L. Foster, and N. Mognard, Analysis of Gauge-measured and Passive Microwave Derived Snow Depth Variations of Snowfields. *J. Hydrometeorology*, 2005 (in press).

Chelton, D.B., M.G. Schlax, M.H. Freilich, and R.F. Milliff, Satellite measurements reveal persistent small-scale features in ocean winds. *Science*, **303**, 978-983, 2004.

Cohen, J., and D. Entekhabi, Eurasian snow cover variability and Northern Hemisphere climate predictability. *Geophysical Research Letters*, **26**, 345-348, 1999.

Comiso, J. C., A rapidly declining perennial sea ice cover in the Arctic. *Geophysical Research Letters*, **29**(20), 1956, doi:10.1029/2002GL015650, 2002.

Derksen, C., A. Walker, and B. Goodison, A comparison of 18 winter seasons of in situ and passive microwave-derived snow water equivalent estimates in Western Canada. *Remote Sensing of Environment*, **88**, 271-282, 2003.

Draper, D.W., and D.G. Long, Evaluating the effect of rain on SeaWinds scatterometer measurements. *Journal of Geophysical Research*, **109**, C02005, doi:10.1029/2002JC001741, 2004a.

Draper, D.W., and D.G. Long, Simultaneous wind and rain retrieval using SeaWinds data. *IEEE Transactions on Geoscience and Remote Sensing*, **42**, 1411-1423, 2004b.

Draper, D.W., and D.G. Long, Assessing the quality of SeaWinds rain measurements. *IEEE Transactions on Geoscience and Remote Sensing*, 42, 1424-1432, 2004c.

Drusch, M., D. Vasiljevic, and P. Viterbo, ECMWF's global snow analysis: an assessment and revision based on satellite observations. *Journal of Applied Metereorology*, **43**, 1282-1294, 2004.

Foster, J.L., C. Sun, J.P. Walker, R.E.J. Kelly, A.T.C. Chang, J. Dong, and H. Powell, Quantifying the uncertainty in passive microwave snow water equivalent observations. *Remote Sensing of Environment*, 2005 (in press).

Furuhama, Y., 2004, GEOSS challenges and Asia-Pacific activities. *Proceedings of IGARSS2004*, 20-24 September 2004, Anchorage, AK, USA, 2004.

Gohin, F., Some active and passive microwave signatures of Antarctic sea ice from mid-winter to spring 1991. *International Journal of Remote Sensing*, **16**, 2031-2054, 1995.

Gohin, F., and A. Cavanie, A first try at identification of sea ice using the three beam scatterometer of ERS-1. *International Journal of Remote Sensing*, **15**, 1221-1228, 1994.

Gohin, F., A. Cavanie, and R. Ezraty, Evolution of the passive and active microwave signatures of a large sea ice feature during its 2.5-year drift through the Arctic Ocean. *Journal of Geophysical Research*, **103**(C4), 8177-8189, 1998.

Grippa, M., N. Mognard, T. Le Toan, and E.G. Josberger, Siberia snow depth climatology derived from SSM/I data using a combined dynamic and static algorithm, *Remote Sensing of Environment*, **93**, 30-41, 2004.

Holloway, G., and T. Sou, Has Arctic sea ice rapidly thinned? *Journal of Climate*, **15**, 1691-1701, 2002.

Howell, S.E.L, J.J. Yackel1, R.A. De Abreu, T. Geldsetzer, and C. Breneman, An evaluation of SeaWinds/QuikSCAT data for the estimation of the decay status of first-year sea ice. *Proceedings of IGARSS2004*, 20-24 September 2004, Anchorage, AK, 2004.

Kelly, R.E.J., A.T.C. Chang, L. Tsang, and J.L. Foster, Development of a prototype AMSR-E global snow area and snow volume algorithm. *IEEE Transactions on Geoscience and Remote Sensing*, **41**(2): 230-242, 2003.

Laxon S., N. Peacock, and D. Smith, High interannual variability of sea ice thickness in the Arctic region. *Nature*, **425** (6961), 947-950, 2003.

Liu, W.T., Progress in scatterometer application. *Journal of Oceanography*, 58, 121-136, 2002.

Lin, I-I, W.T. Liu, C.-C. Wu, G. T.F. Wong, C.Hu, Z. Chen, W.-D. Liang, Y. Yang, and K.-K. Liu, New evidence for enhanced ocean primary production triggered by tropical cyclone. *Geophysical Research Letters*, **30**(13), 1718, doi:10.1029/ 2003GL017141, 2003.

Liu, W.T., and K.B. Katsaros, Air-Sea Flux from Satellite Data. *Ocean Circulation and Climate*. G. Siedler. J. Church, and J. Gould (eds), Ch. 3.4, 1173-1179, Academic Press, New York, 2001.

Liu, W.T., and P.P. Niiler, Determination of monthly mean humidity in the atmospheric surface layer over oceans from satellite data. *Journal of Physical Oceanography,* **14***,* 1451-1457, 1984.

Liu, W.T. and W. Tang, Oceanic Influence on the precipitation in India and China as observed by TRMM and QuikSCAT. *Proceedings of TRMM Conference*, 2004.

Liu, W.T., and W. Tang, Estimating moisture transport over ocean using spacebased observations from space. *Journal of Geophysical Research*, 2005 (in press).

Liu, W.T., H. Hu, and S. Yueh, Interplay between wind and rain observed in Hurricane Floyd. *Eos, Transactions of American Geophysical Union*, **81**, 253 & 257, 2000.

Liu, A. K., Y. Zhao, and W. T. Liu, Sea-ice motion derived from satellite agrees with buoy observations. *Eos, Transactions, American Geophysical Union*, **79**(30), 353-359, 1998.

Liu, A. K., Y. Zhao, and S. Y. Wu, Arctic sea ice drift from wavelet analysis of NSCAT and special sensor microwave imager data. *Journal of Geophysical Research*, **104**, (C5), 11,529-11,538, 1999.

Lo, F., and M. Clark, Relationships between spring snow mass and summer precipitation in the southwestern United States associated with the North American monsoon system. *Journal of Climate*, **15**, 1378-1385, 2002.

Markus, T., D. J. Cavalieri, A. Gasiewski, M. Klein, M. Sturm, J. Maslanik, J. Stroeve, and J. Heinrichs, Comparisons of Arctic in-situ snow and ice data with airborne passive microwave measurements. *Proceedings of IGARSS2004*, 20-24 September 2004, Anchorage, AK, USA, 2004.

Milliff, R.F., J. Morzel, D.B. Chelton, and M.H. Freilich, Wind stress curl and wind stress divergence biases from rain effects on QSCAT surface wind retrievals. *J. Atmosphere and Oceanic Technology*, **21**, 1216-1231, 2004.

Nghiem, S.V., Observations of Arctic environmental change, *Proceeding of IGARSS2004*, 20-24 September 2004, Anchorage, AK, 2004.

Nghiem, S.V., and W.Y. Tsai, Global snow cover monitoring with spaceborne Ku-band scatterometer. *IEEE Transactions on Geoscience and Remote Sensing*, **39**, 2118-2134, 2001.

Pfirman, S., W. Haxby, H. Eicken, M. Jeffries, and D. Bauch, Drifting Arctic sea ice archives changes in ocean surface conditions. *Geophysical Research Letters*, **31**, L19401, doi:10.1029/2004GL020666, 2004.

Rothrock, D. A., Y. Yu, and G. A. Maykut, Thinning of the Arctic sea ice cover. *Geophysical Research Letters*, **26**, 3469-3472, 1999.

Schlosser, C.A., and D.M. Mocko, Impact of snow conditions in spring dynamical seasonal prediction. *Journal of Geophysical Research*, doi: 10.1029/ 2002JD003113, 2003.

Sun, C., J.P. Walker, and P.R. Houser, A methodology for snow data assimilation in a land surface model. *Journal of Geophysical Research*, doi: 10.1029/ 2003JD003765, 2004.

Tsang, L., C. Chen, A.T.C. Chang, J. Guo, and K. Ding, Dense media radiative transfer theory based on quasicrystalline approximation with applications to passive microwave remote sensing of snow. *Radio Science*, **35**, 731-749, 2000.

Weissman, D.E., M.A. Bourassa, and J. Tongue, Effects of rain-rate and wind magnitude on SeaWinds scatterometer wind speed errors. *Journal Atmospheric and Oceanic Technology*, **19**(5), 738-746, 2002.

Weissman, D.E., M.A. Bourassa, J.J. O'Brien and J. Tongue, Calibrating the QuikSCAT/ SeaWinds radar for measuring rain rate over the oceans. *IEEE Transactions on Geoscience and Remote Sensing*, **41**(12), 2814-2820, 2003.

Weissman, D.E., M.A. Bourassa, and S.L. Durden, Corrections to the SeaWinds Scatterometer Wind Vectors by Removing the Effects of Rain from the NRCS. *Proceedings of IGARSS2004*, 20-24 September 2004, Anchorage, AK, USA, 2004.

Xie, X., and W.T. Liu, Hydrological budget in the Tropical Pacific. *Proceedings of 16th Conference on Climate Variability and Change*, American Meteorological Society, Boston, 2005.

Xie, S.-P., W.T. Liu, Q. Liu, and M. Nonaka, Far-reaching effects of the Hawaiian Islands on the Pacific Ocean-atmosphere system. *Science*, **292**, 2057-2060, 2001.

Xie, S.-P., J. Hafner, Y. Tanimoto, W.T. Liu, H. Tokinaga, and H. Xu, Bathymetric effect on the winter sea surface temperature and climate of the Yellow and East China Seas. *Geophysical Research Letters*, **29**, 2228, doi: 10.1029/2002GL015884, 2002.

Zhao, Y., A. K. Liu, and D. Long, Validation of sea ice motion from QuikSCAT with those from SSM/I and buoy. *IEEE Transactions on Geoscience and Remote Sensing*, **40**,1241-1246, 2002.